

# Detectability of the chiral gravitational wave background from audible axions with the LISA-Taiji network

Hong Su<sup>1,5,6</sup>, Baoyu Xu<sup>2,7</sup>, Ju Chen<sup>3,5,\*</sup>, Chang Liu<sup>4,†</sup> and Yun-Long Zhang<sup>2,1‡</sup>

<sup>1</sup> *School of Fundamental Physics and Mathematical Sciences,*

*Hangzhou Institute for Advanced Study, UCAS, Hangzhou 310024, China.*

<sup>2</sup> *National Astronomical Observatories, Chinese Academy of Sciences, Beijing 100101, China*

<sup>3</sup> *International Center for Theoretical Physics Asia-Pacific (ICTP-AP),*

*University of Chinese Academy of Sciences, Beijing 100190, China*

<sup>4</sup> *Center for Gravitation and Cosmology, College of Physical Science and Technology, Yangzhou University, Yangzhou, 225009, China*

<sup>5</sup> *Taiji Laboratory for Gravitational Wave Universe (Beijing/Hangzhou), University of Chinese Academy of Sciences, Beijing 100049, China*

<sup>6</sup> *CAS Key Laboratory of Theoretical Physics, Institute of Theoretical Physics, Chinese Academy of Sciences, Beijing 100190, China. and*

<sup>7</sup> *School of Astronomy and Space Science, University of Chinese Academy of Sciences, Beijing 100049, China.*

(Dated: March 27, 2025)

The chiral gravitational wave background (GWB) can be produced by axion-like fields in the early universe. We perform parameter estimation for two types of chiral GWB with the LISA-Taiji network: axion-dark photon coupling and axion-Nieh-Yan coupling. We estimate the spectral parameters of these two mechanisms induced by axion and determine the normalized model parameters using the Fisher information matrix. For highly chiral GWB signals that we choose to analyze in the mHz band, the normalized model parameters are constrained with a relative error less than 6.7% (dark photon coupling) and 2.2% (Nieh-Yan coupling) at the one-sigma confidence level. The circular polarization parameters are constrained with a relative error around 21% (dark photon coupling) and 6.2% (Nieh-Yan coupling) at the one-sigma confidence level.

## CONTENTS

I. Introduction	1
II. Audible Axions and Chiral GW Background	2
A. Chiral GWB from Dark Photon coupling	2
B. Chiral GWB from Nieh-Yan coupling	3
III. Network of Space-based GW detectors	4
A. Noise and sensitivity of the detectors	4
B. LISA-Taiji cross-correlations	6
IV. Fisher Matrix Analysis	6
A. GW spectral parameters	7
B. Normalized model parameters	7
V. Conclusion	10
Acknowledgement	10
A. Response functions of GWs	10
1. Polarization tensor bases	11
2. Quadratic response functions	11
3. The AET bases	12
References	12

## I. INTRODUCTION

The direct detection [1] of gravitational waves (GWs) by the Laser Interferometer Gravitational-Wave Observatory (LIGO) [2] has offered a novel method for exploring the physics of the early Universe [3–6]. GWs produced by axions or axion-like particles (ALPs), especially the stochastic gravitational wave background (SGWB) from the early Universe, enable the detection of new physics beyond the Standard Model and provide insights into the early Universe [7–13]. Axions were originally introduced to address the strong CP problem within the Standard Model [14–19]. While numerous mechanisms exist for the production of axions in the early Universe [20, 21], enabling a wide range of dark matter axion masses, these mechanisms may also contribute to various cosmological phenomena [22].

Axions and ALPs typically have weak couplings to photons or other Standard Model particles, making them difficult to detect directly [23, 24]. Moreover, these particles have been proposed to address other Standard Model and cosmological challenges, such as resolving the electroweak hierarchy problem [25, 26], serving as dark matter (DM) candidates [23, 27, 28] or inflatons [29], and being present in string theory frameworks [30]. The audible axions model proposed in Refs. [31, 32] describes the coupling between axions and dark photons (gauge bosons), in which dark photons experience tachyonic instability when axions oscillate. The model postulates that axions or ALPs possess large initial velocities, enabling the generation of detectable GW signals even with

\* [chenju@ucas.ac.cn](mailto:chenju@ucas.ac.cn)

† [liuchang@yzu.edu.cn](mailto:liuchang@yzu.edu.cn)

‡ [zhangyunlong@nao.cas.cn](mailto:zhangyunlong@nao.cas.cn)

small decay constants. This process results in the generation of an SGWB in the early Universe, allowing us to detect these particles, which carry chirality. Parity violation will serve as a powerful observable for distinguishing cosmological background GWs from astrophysical ones [33]. Probing axion dark matter through future space-based gravitational-wave detectors will enable the exploration of broader parameter space for axions and ALPs. Except for the ground-based gravitational-wave observatories [34, 35], forthcoming space-based missions hold the potential to probe axion-like dark matter directly [36–38].

The SGWB arises from the superposition of GWs produced by a large number of independent sources [39]. It exhibits stochasticity and has a signal strength that is relatively weak compared to the total intensity sensitivity of detectors, categorizing it as a weak signal, and methods for its detection have been developed [40]. Due to the stochastic and uncorrelated nature of the general generation process, the SGWB is assumed to be unpolarized. However, parity violation in gravity, such as the Chern-Simons coupling [41, 42] and the Nieh-Yan coupling in teleparallel equivalent of general relativity (TEGR) [43–51], can modify the generation and propagation of gravitational waves, leading to a circularly polarized SGWB. The chirality of GWs can be effectively measured within the frequency bands of several detectors, including ground-based detectors [52–54], space-based instruments such as LISA [55] and Taiji [56], and through observations of the Cosmic Microwave Background (CMB) [57, 58].

LISA (Laser Interferometer Space Antenna) is a triangular GW detector in the orbit around the Sun, which is expected to be launched in the 2030s, with an arm length of  $L = 2.5 \times 10^9$  m [59]. Taiji is similar to LISA but has an arm length of  $L = 3 \times 10^9$  m [60]. Due to their planar configuration, individual detectors are insensitive to the chiral signatures of GWs. For an isotropic SGWB, the detection of its circular polarization requires the correlation of two non-coplanar gravitational wave detectors [61]. Therefore, a network of detectors is necessary, such as ground-based networks [62, 63] or the space-based network LISA-Taiji [56, 64–70], which can enhance the detection of the circular polarization of the SGWB. Furthermore, space-based GW detector networks also provide numerous other advantages, including improved gravitational wave polarization measurements [71], enhanced parameter estimation for Galactic binaries [72], better sky localization accuracy [73, 74], more accurate localization of massive binaries [75], detection of black hole formation mechanisms [76], increased detection capabilities for stellar binary black holes [77], and increased precision of GW standard sirens and cosmological parameter estimation [78–80].

To evaluate the detection capability of the LISA-Taiji network for chiral gravitational wave background (GWB), we estimate the spectral parameters and normalized model parameters of the chiral GWB generated

by early cosmic axions using the Fisher information matrix. Additionally, we perform a Fisher analysis based on the fitted SGWB energy density spectrum from the dark photon coupling model [81] and broken power-law spectrum from the Nieh-Yan coupling model [51].

The paper is organized as follows. In Sec. II, we briefly introduce how axions generate chiral gravitational waves through coupling with dark photons or the Nieh-Yan term, and present the energy density spectrum of the resulting gravitational waves, along with fitted templates and parameters. In Sec. III, we describe the configuration of the space-based GW detector network and calculate its response to GWs. In Sec. IV, we derive the Fisher information matrix and determine the parameters for two different GW energy spectra with the network. In Sec. V, we present the conclusion and discussion. The calculations in this work are performed using the Python packages `numpy` and `scipy`, and the plots are generated using `matplotlib` and `GetDist`.

## II. AUDIBLE AXIONS AND CHIRAL GW BACKGROUND

Several mechanisms that produce chiral GWs from audible axions have been explored in prior research. One is the coupling of axion to dark photon [31, 81, 82], while the other involves axion coupling to the parity-violating gravity such as Chern-Simons [83–85] and Nieh-Yan modified gravity [43–51]. The former just generates chiral GWs mediated by dark photons, while the latter can produce GWs directly and efficiently. In this section, we explore the GW spectrum template and fitting parameters produced by these mechanisms.

### A. Chiral GWB from Dark Photon coupling

The chiral GWB can be generated through the asymmetrical production of dark photons [31, 81, 82]. In this mechanism, the total action can be expressed as

$$S_{\text{DP}} = \int d^4x \sqrt{-g} \left[ \frac{M_p^2}{2} R - \frac{1}{4} X_{\mu\nu} X^{\mu\nu} + \frac{\alpha_X}{4f_X} \phi X_{\mu\nu} \tilde{X}^{\mu\nu} - \frac{1}{2} \partial_\mu \phi \partial^\mu \phi - V(\phi) \right]. \quad (1)$$

Here,  $f_X$  is the decay constant of the axion,  $\alpha_X$  is the coupling coefficient and  $V(\phi) = m^2 f_X^2 \left[ 1 - \cos\left(\frac{\phi}{f_X}\right) \right]$  is the cosine-like potential with the axion mass  $m$ . The third term in this action leads to a nontrivial dispersion relation for the helicities of dark photons, which takes the form  $\omega_{X,\pm}^2 = k_X^2 \mp k_X \frac{\alpha_X}{f_X} \phi'$ . This indicates that the asymmetric production of dark photons results in an oscillating stress-energy distribution that sources gravitational waves.

Previous studies provide a well-fitting curve for the chiral gravitational wave energy density spectrum produced

by dark photons. For the SGWB template, a suitable ansatz is [81]

$$\tilde{\Omega}_{\text{GW}}(\tilde{f}_p) = \frac{\mathcal{A}_s \left( \tilde{f}_p / f_s \right)^p}{1 + \left( \tilde{f}_p / f_s \right)^p \exp \left[ \gamma (\tilde{f}_p / f_s - 1) \right]}, \quad (2)$$

where  $\tilde{\Omega}_{\text{GW}} \equiv \Omega_{\text{GW}}(f) / \Omega_{\text{GW}}(f_p)$  represents the normalized GW energy density,  $f_p$  denotes the peak frequency.  $f$  denotes the GW frequency and  $\tilde{f}_p \equiv f / f_p$  is the dimensionless normalized frequency. Moreover,  $\mathcal{A}_s, f_s, \gamma, p$  are the fitting parameters.

From the derivation in [31], the peak amplitude and peak frequency of the GW spectrum, at the time of GW emission, are given by  $f_p \simeq (\alpha_X \theta)^{2/3} m$ ,  $\Omega_{\text{GW}}(f_p) \simeq \left( \frac{f_X}{M_P} \right)^4 \left( \frac{\theta^2}{\alpha_X} \right)^{4/3}$ . Here,  $\theta$  is the initial misalignment angle and  $M_P \simeq 2.4 \times 10^{18}$  GeV is the reduced Planck mass. Considering the expansion of the Universe, which leads to redshifting, these quantities become [31]

$$f_p^0 \simeq (\alpha_X \theta)^{2/3} T_0 \left( \frac{g_{s,0}}{g_{s,*}} \right)^{1/3} \left( \frac{m}{M_P} \right)^{1/2}, \quad (3)$$

$$\Omega_{\text{GW}}^0(f_p^0) \simeq 1.67 \times 10^{-4} g_{s,*}^{-1/3} \left( \frac{f_X}{M_P} \right)^4 \left( \frac{\theta^2}{\alpha_X} \right)^{4/3}. \quad (4)$$

Here, we choose the effective number of relativistic degrees of freedom  $g_{s,*} = 106.75$ , because the mechanism occurs near the QCD phase transition.  $g_{s,0} = 3.938$  is the effective relativistic degree of freedom today when the temperature  $T_0 = 2.35 \times 10^{-13}$  GeV. Based on the equations above, to produce detectable GW signals within the mHz frequency band, we adopt the following parameter values:  $m = 1.0 \times 10^{-2}$  eV,  $f_X = 1.0 \times 10^{17}$  GeV,  $\alpha_X = 55$ , and  $\theta = 1.2$ , as proposed by [31].

### B. Chiral GWB from Nieh-Yan coupling

The chiral GWB can also be generated through an axion-like mechanism that couples to the Nieh-Yan term, resulting in the direct and efficient production of chiral GWB during the radiation-dominated epoch [51]. This generation arises from the tachyonic instability of gravitational perturbations induced by the Nieh-Yan term. The total action for this mechanism can be written as

$$S_{\text{NY}} = \int d^4x \sqrt{-g} \left[ -\frac{M_{\text{P}}^2}{2} \hat{T} + \frac{\alpha_T M_{\text{P}}^2}{4f_T} \phi \hat{T}_{A\mu\nu} \tilde{T}^{A\mu\nu} - \frac{1}{2} \partial_\mu \phi \partial^\mu \phi - V(\phi) \right]. \quad (5)$$

Here,  $\hat{T}$  is the torsion scalar, which is dynamically equivalent to the Ricci scalar in general relativity. Similar to the action in Eq.(1),  $f_T$  is the axion decay constant,  $\alpha_T$  is the coupling coefficient and  $V(\phi)$  represents the cosine-like potential. The second term in Eq.(5) can also lead

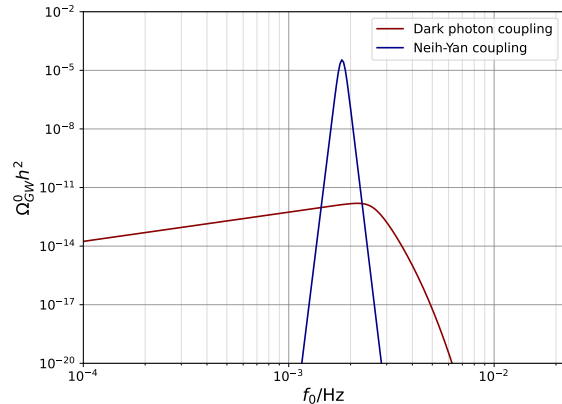


FIG. 1: The broken power-law fitted curves of the SGWB for the dark photon (red) and Nieh-Yan (blue) coupling models, each using two parameter sets as described in Sec. II A and II B.

to a non-trivial dispersion relation for the GW helicities, given by  $\omega_{T,\pm}^2 = k_T^2 \pm \frac{\alpha_T \phi'}{f_T M_P^2} k_T$ . The  $k_T$  here is the wave vector for GWs, indicating that the last term produces an effect analogous to the term  $\frac{\alpha_X}{4f_X} \phi X_{\mu\nu} \tilde{X}^{\mu\nu}$  in the dark photon case.

Specifically, when the axion field oscillates, one of the GW helicities will have a range of modes with imaginary frequencies, resulting in a tachyonic instability that drives exponential growth. Since the growth rate is related to helicities, the left-handed and right-handed GWs are generated asymmetrically, ultimately leading to chiral GWB. In [51], the broken power-law template provides a better fit for the GW spectrum in this model, which can be written as

$$\tilde{\Omega}_T = \left( \tilde{f}_c \right)^{\alpha_1} \left[ 1 + 0.75 \left( \tilde{f}_c \right)^\Delta \right]^{\frac{(\alpha_2 - \alpha_1)}{\Delta}}. \quad (6)$$

Here,  $\tilde{\Omega}_T \equiv \Omega_T(f) / \Omega_c$ , where  $\Omega_c$  is the characteristic energy density.  $\tilde{f}_c \equiv f / f_c$  is the dimensionless normalized frequency with the characteristic frequency  $f_c$ . Moreover,  $\alpha_1, \alpha_2$  and  $\Delta$  are fitting parameters.

In this equation, the characteristic frequency today,  $f_c^0$ , can be expressed in terms of physical parameters as

$$f_c^0 = 0.7125 \text{ mHz} \left( \frac{100}{g_{s,*}} \right)^{1/2} \left( \frac{9}{14} \alpha_T \theta \right)^{2/3} \left( \frac{m}{\text{eV}} \right)^{1/2}. \quad (7)$$

Here, we also choose  $g_{s,*} = 106.75$ , as this mechanism occurs near the QCD phase transition. The characteristic energy density  $\Omega_c^0$  can similarly be written in terms of physical parameters as

$$\Omega_c^0 = \frac{\theta^2 f_T^2 / 2}{3M_P^2} \frac{m^2}{H_{\text{osc}}^2} \simeq \left( \frac{\theta f_T}{M_P} \right)^2. \quad (8)$$

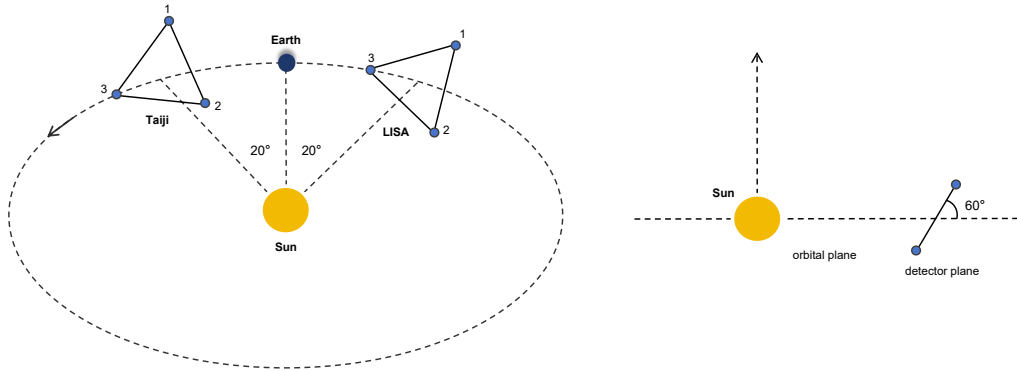


FIG. 2: The configuration of the LISA-Taiji joint network, including the spacecraft numbering scheme. LISA orbits 20 degrees behind the Earth, while Taiji precedes the Earth by the same angle. Both detector planes are inclined at 60 degrees relative to the ecliptic plane.

For the Nieh-Yan coupling model, we choose the following parameters to generate detectable gravitational wave signals in the mHz band:  $m = 0.1$  eV,  $f_T = 1.0 \times 10^{17}$  GeV,  $\alpha_T = 35.61$ , and  $\theta = 1$  [51].

In Fig. 1, we present the broken power-law fit curves of the SGWB spectrum generated by the dark photon coupling model and the Nieh-Yan coupling model.

### III. NETWORK OF SPACE-BASED GW DETECTORS

In this section, we adopt the commonly used orbits of LISA and Taiji, combining them to evaluate their effectiveness in detecting the SGWB. We establish the coordinate system in the Solar System Barycentric Coordinate System (SSB). LISA trails the Earth by 20 degrees, and Taiji leads by the same degree, with both detector planes tilted 60 degrees relative to the ecliptic plane. The LISA-Taiji network configuration is displayed as Fig. 2.

#### A. Noise and sensitivity of the detectors

Each detector contains three interferometers that simultaneously detect the Doppler shift induced by GWs. The data stream of Time-Delay Interferometry (TDI) channel  $i$  is given by

$$d_i(t) = s_i(t) + n_i(t), \quad (9)$$

where  $s_i(t)$  represents the signal and  $n_i(t)$  denotes the instrumental noise. In general, it is more convenient to work in the frequency domain

$$\tilde{d}_i(f) = \int_{-T/2}^{T/2} dt e^{2\pi i f t} d_i(t), \quad (10)$$

where  $T$  represents the observation time. In this paper, we assume that the noise is Gaussian and uncorrelated. The respective correlations of the signal and noise in the frequency domain can be expressed as

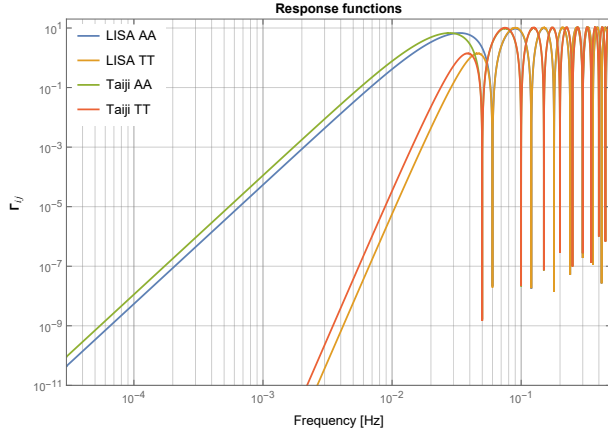
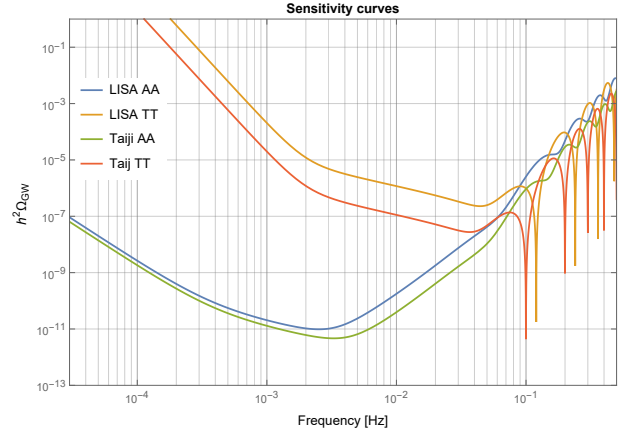
$$\begin{aligned} \langle \tilde{s}_i(f) \tilde{s}_j^*(f') \rangle &= \frac{1}{2} S_{ij}(f) \delta(f - f'), \\ \langle \tilde{n}_i(f) \tilde{n}_j^*(f') \rangle &= \frac{1}{2} N_i(f) \delta_{ij} \delta(f - f'), \end{aligned} \quad (11)$$

where  $S_{ij}(f)$  and  $N_i(f)$  are the one-sided signal and noise power spectral density (PSD), respectively. Assuming independent TDI channel noises (e.g., in the A, E, T combination, which are the optimal TDI variables for LISA-like detectors),  $S_{ij}(f)$  can be expressed as

$$\begin{aligned} S_{ij}(f) &= \sum_{\lambda} P_{\lambda}(f) \Gamma_{ij}^{\lambda}(f) = \sum_{\lambda} P_{\lambda}(f) \times \\ &\left[ (2\pi k L_i) (2\pi k L_j) W(k L_i) W^*(k L_j) \tilde{\Gamma}_{ij}^{\lambda}(f) + \text{h.c.} \right]. \end{aligned} \quad (12)$$

Here,  $k = f/c$ ,  $\lambda = L$  or  $R$  identifies left- and right-handed polarizations,  $L_i$  and  $L_j$  are the detector arm lengths,  $\Gamma_{ij}^{\lambda}(f)$  is the full detector response function and  $P_{\lambda}(f)$  is the GW power spectrum. The function  $W(kL)$  represents the phase delay due to the detector arm length, as detailed in Appendix A2.  $\tilde{\Gamma}_{ij}^{\lambda}(k)$  denotes the geometrical contribution to the detector response function for the correlation between channels  $i$  and  $j$ , as detailed in equation (A11).

In this work, we adopt the standard two-parameter noise model used for LISA, which accounts for the two dominant noise sources in space-based GW detectors: acceleration (acc) noise and Optical Measurement System (OMS) noise. For Taiji, we use a similar noise model with distinct parameters  $A_{\text{acc}}$  and  $A_{\text{OMS}}$ . The acceleration noise power spectrum  $P_{\text{acc}}(f)$  and OMS noise power

(a) The self-correlation response functions  $\Gamma_{ij}(f)$ .

(b) Sensitivity curves for the total intensity of GWs.

FIG. 3: (a) The self-correlation response functions  $\Gamma_{ij}$  in (A14) of a single detector, for the respective TDI channels of LISA and Taiji, where the E channel has the same result as the A channel. (b) The sensitivity curves for the total intensity of GWs in Eq. (18) for the self-correlation of the respective channels of LISA and Taiji, where again the E-channel has the same results as the A-channel.

spectrum  $P_{\text{OMS}}(f)$  are given by [86, 87]

$$P_{\text{acc}}(f) = A_{\text{acc}}^2 \left[ 1 + \left( \frac{0.4\text{MHz}}{f} \right)^2 \right] \left( \frac{2\pi f}{c} \right)^2 \times \left[ 1 + \left( \frac{f}{8\text{MHz}} \right)^4 \right] \left( \frac{1}{2\pi f} \right)^4, \quad (13)$$

$$P_{\text{OMS}}(f) = A_{\text{OMS}}^2 \left[ 1 + \left( \frac{2\text{mHz}}{f} \right)^4 \right] \left( \frac{2\pi f}{c} \right)^2. \quad (14)$$

Here,  $A_{\text{acc}}$  and  $A_{\text{OMS}}$  are the amplitudes of the acceleration noise and the OMS noise, respectively. For the two detectors, the noise amplitude parameters for LISA [88] and Taiji [65, 89, 90] are listed in Table I.

	$A_{\text{OMS}}$	$A_{\text{acc}}$	$L$
LISA	15 pm/ $\sqrt{\text{Hz}}$	3 fm/s <sup>2</sup> / $\sqrt{\text{Hz}}$	2.5 Gm
Taiji	8 pm/ $\sqrt{\text{Hz}}$	3 fm/s <sup>2</sup> / $\sqrt{\text{Hz}}$	3.0 Gm

TABLE I: Noise amplitude spectral density parameters and arm lengths for different space-based GW detectors.

For convenience, we define the detector's characteristic frequency as  $f_* \equiv c/2\pi L$ . The power spectral density of the noise for a single detector channel is then given by [12, 91]

$$N_A(f) = N_E(f) = 8 \sin^2 \left( \frac{f}{f_*} \right) \left\{ 4 \left[ 1 + \cos \left( \frac{f}{f_*} \right) + \cos^2 \left( \frac{f}{f_*} \right) \right] \times P_{\text{acc}}(f) + \left[ 2 + \cos \left( \frac{f}{f_*} \right) \right] \times P_{\text{OMS}}(f) \right\}, \quad (15)$$

and

$$N_T(f) = 16 \sin^2 \left( \frac{f}{f_*} \right) \left\{ 2 \left[ 1 - \cos \left( \frac{f}{f_*} \right) \right]^2 \times P_{\text{acc}}(f) + \left[ 1 - \cos \left( \frac{f}{f_*} \right) \right] \times P_{\text{OMS}}(f) \right\}, \quad (16)$$

where the subscripts A, E, and T denote the noise-orthogonal TDI channels A, E, and T, respectively.

To directly compare incident GW signals with detector noise, we define the strain sensitivity of total intensity for all GW modes as [12]

$$P_{N,ii}(f) = \frac{N_i(f)}{\Gamma_{ii}(f)}, \quad (17)$$

where  $\Gamma_{ii}(f)$  represents the sky-averaged response functions of individual TDI channels, which can be calculated via Eq. (A14). The corresponding total intensity, in GW energy density units, is given by:

$$h^2 \Omega_{N,ii}(f) = \frac{4\pi^2 f^3}{3(H_0/h)^2} P_{N,ii}(f), \quad (18)$$

where  $H_0 = h 100 \text{ km s}^{-1} \text{ Mpc}^{-1}$  is the value of the present-day Hubble parameter and  $h = 0.67$  is the dimensionless Hubble parameter. Fig. 3b shows the total intensity sensitivity curves for the A and E channels of both LISA and Taiji. Similarly, the SGWB adopts a similar notation, with  $P_{N,ij}$  replaced by the signal PSD [56]

$$h^2 \Omega_{\text{GW}}^\lambda(f) = \frac{4\pi^2 f^3}{3(H_0/h)^2} P_\lambda(f). \quad (19)$$

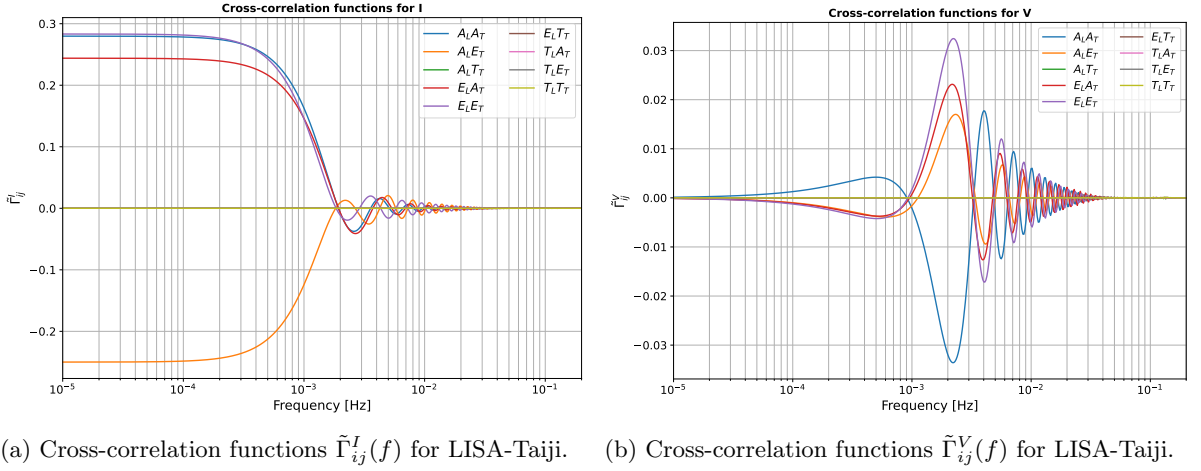


FIG. 4: Cross-correlation functions  $\tilde{\Gamma}_{ij}^\lambda(f)$  in Eq. (A11) between the TDI channels of LISA and Taiji, for Stokes parameter  $I$  in (a) and  $V$  in (b).

### B. LISA-Taiji cross-correlations

We use the Stokes parameters  $I(f)$  and  $V(f)$  to characterize the polarization of the SGWB in the cross-correlated detector data stream. They are defined as

$$I(f) = P_R(f) + P_L(f), \quad V(f) = P_R(f) - P_L(f). \quad (20)$$

Here,  $I$  represents the total intensity of the GW, while  $V$  quantifies the difference between right-handed and left-handed circular polarization intensities. Parity-violating effects in the early Universe may give rise to a nonzero value of  $V$ . By using detectors to measure it, we can extract information about the circular polarization of GWs. We can express GW power spectral density  $S_{ij}$  as

$$S_{ij}(f) = I(f)\Gamma_{ij}^I(f) + V(f)\Gamma_{ij}^V(f), \quad (21)$$

where  $\Gamma_{ij}^I(f)$  and  $\Gamma_{ij}^V(f)$  are the overlap reduction functions for intensity and circular polarization components, quantifying the correlated response between TDI channels  $i$  and  $j$ . These functions are defined as:

$$\begin{aligned} \Gamma_{ij}^I(f) &= \frac{\Gamma_{ij}^R(f) + \Gamma_{ij}^L(f)}{2}, \\ \Gamma_{ij}^V(f) &= \frac{\Gamma_{ij}^R(f) - \Gamma_{ij}^L(f)}{2}. \end{aligned} \quad (22)$$

Thus, the power spectral density in Eq. (12) for  $\tilde{\Gamma}_{ij}^\lambda(f)$  can be reformulated using the Stokes parameters  $I$  and  $V$ , with  $\lambda = I, V$ . By cross-correlating the signals from LISA and Taiji channels, we can extract nonzero  $\tilde{\Gamma}_{ij}^\lambda(f)$  values. The  $I$  and  $V$  components resulting from this cross-correlation of all TDI channels between LISA and Taiji are presented in Fig. 4.

Additionally, we introduce the circular polarization parameter as

$$\Pi(f) = \frac{V(f)}{I(f)}. \quad (23)$$

The correlation between the outputs of different detectors can be expressed as:

$$\langle \mathcal{C}_{ij} \rangle = \langle \hat{d}_i \hat{d}_j \rangle = \frac{1}{2} [\Gamma_{ij}^I(f)I(f) + \Gamma_{ij}^V(f)V(f)]. \quad (24)$$

Assuming that the noise is Gaussian, the likelihood function of the signal model is [92]

$$\begin{aligned} \mathcal{L} &= p(\mathcal{C} | \theta) \\ &\propto \exp \left\{ -\frac{T_{\text{obs}}}{2} \sum_{\kappa} \int_0^{\infty} df \frac{[2\mathcal{C}_{\kappa} - (\Gamma_{\kappa}^I I + \Gamma_{\kappa}^V V)]^2}{N_{\kappa}^2(f)} \right\}, \end{aligned} \quad (25)$$

where  $\kappa = \{A_L - A_T, A_L - E_T, E_L - A_T, E_L - E_T\}$  represent the independent channel pairs of LISA and Taiji. With  $A_L$  and  $E_L$  denoting the LISA channels and  $A_T$  and  $E_T$  corresponding to the Taiji channels.  $T_{\text{obs}}$  denotes the effective observation time, which is set to 3 years in this work. The noise term  $N_{\kappa}(f)$  is defined as  $N_{\kappa}(f) = \sqrt{N_i(f)N_j(f)}$ . For strong GW signal, such as an SGWB with a large signal-to-noise ratio (SNR),  $N_{\kappa}^2(f)$  in (25) is replaced by [92–94]

$$M_{ij}(f) = (N_i + \Gamma_{ii}I)(N_j + \Gamma_{jj}I) + (\Gamma_{ij}^I I + \Gamma_{ij}^V V)^2. \quad (26)$$

### IV. FISHER MATRIX ANALYSIS

In this section, we employ Fisher matrix analysis to estimate the measurement accuracy of the GW spectral parameters. The Fisher matrix is given by as [56, 92]

$$F_{ab} = -\sum_{\kappa} 4T_{\text{obs}} \int_0^{\infty} df \frac{\frac{\partial \langle C_{\kappa} \rangle}{\partial \theta_a} \frac{\partial \langle C_{\kappa} \rangle}{\partial \theta_b}}{N_{\kappa}^2(f)}, \quad (27)$$

where  $\theta_a$  and  $\theta_b$  are the model parameters. The term  $C_{\kappa}$  is the correlation of the observed data between the

$\kappa$  channel sets, and  $N_\kappa(f)$  represents the signal variance caused by noise. For the frequency integration, we take the lower cutoff at  $10^{-5}$  Hz and the upper cutoff at  $10^{-1}$  Hz. In this study, we assume a frequency-independent circular polarization parameter  $\Pi(f) = \Pi$  and derive the Fisher matrix expression for the GW model parameters as follows.

By substituting the signal Eq. (19), the circular polarization parameter in Eq. (23), and Eq. (24), we have

$$F_{ab} = 4T_{\text{obs}} \left( \frac{3H_0^2}{4\pi^2} \right)^2 \times \sum_{\kappa} \int_0^\infty df \frac{(\Gamma_\kappa^I + \Pi \Gamma_\kappa^V)^2 \partial_{\theta_a} \Omega(f) \partial_{\theta_b} \Omega(f)}{f^6 N_\kappa^2}, \quad (28)$$

with  $a$  and  $b$  indicate both parameters of the GW model. For example, when one parameter is  $\Pi$  and the other is a GW model parameter

$$F_{a\Pi} = 4T_{\text{obs}} \left( \frac{3H_0^2}{4\pi^2} \right)^2 \times \sum_{\kappa} \int_0^\infty df \frac{\Gamma_\kappa^V (\Gamma_\kappa^I + \Pi \Gamma_\kappa^V) \Omega(f) \partial_{\theta_a} \Omega(f)}{f^6 N_\kappa^2}. \quad (29)$$

When both parameters in the Fisher matrix are  $\Pi$

$$F_{\Pi\Pi} = 4T_{\text{obs}} \left( \frac{3H_0^2}{4\pi^2} \right)^2 \sum_{\kappa} \int_0^\infty df \frac{(\Gamma_\kappa^V)^2 \Omega(f)^2}{f^6 N_\kappa^2}. \quad (30)$$

### A. GW spectral parameters

We selected the spectral parameters of the GW template for parameter estimation, as detailed in Table II, and the results from the Fisher analysis of the GW energy density spectrum template (2) for audible axion are illustrated in Fig. 5.

$A_s$	$f_s$	$\gamma$	$p$	$\Pi$
6.3	2.0	12.9	1.5	0.9999

TABLE II: Parameter values for the broken power-law template (2) for the dark photon coupling model.

For the dark photon coupling model, the uncertainties in the parameter estimates are illustrated graphically, encompassing four spectral parameters  $\{A_s, f_s, \gamma, p\}$  and the circular polarization parameter  $\Pi$ . The confidence ellipses indicate that the true parameter values lie within the inner ellipse at a  $1\sigma$  confidence level and within the outer ellipse at a  $2\sigma$  confidence level. At the  $1\sigma$  confidence level, the relative errors are less than 62.0% for spectral parameters and less than 23.0% for  $\Pi$ . The elongation of the confidence ellipses reflects the strength of the correlation among spectral parameters,

with more elongated ellipses indicating stronger correlations. Specifically,  $p$  and  $A_s$  exhibit a strong correlation. Additionally, the  $\Pi$  is negatively correlated with  $A_s, p$ , shows a weak negative correlation with  $\gamma$  and is independent of  $f_s$ . In Figs. 5, 6, 7a, and 7b, the gray solid line represents the fiducial value  $\Pi = 1$ , representing a fully polarized state. The gray shaded areas in the corner plots correspond to regions of the parameter space where  $\Pi > 1$ , which is theoretically unacceptable.

For the broken power-law template in the Nieh-Yan coupling models, we also have selected the spectral parameters as shown in Table III, with the corresponding Fisher analysis results presented in Fig. 6. The direct coupling of the axion to the gravitational field in Eq.(5) and the parameter choices in Table III result in a strong signal, making the variance assumption invalid. Therefore, the noise term  $N_\kappa^2$  in our Fisher matrix is replaced by  $M_\kappa(f)$  in Eq. (26). The Fisher analysis results for the GW energy density spectrum in the Nieh-Yan coupling model are shown in Fig. 6. At the  $1\sigma$  confidence level, the relative errors are less than 31.8% for spectral parameters and less than 6.7% for  $\Pi$ .  $\Omega_c$  and  $f_c$  exhibit relatively independent errors, while other spectral parameters show significant correlations. Furthermore, the circular polarization parameter  $\Pi$  exhibits a negative correlation with  $\Omega_c$  and  $f_c$ , a statistically weak correlation with  $\alpha_1$  and  $\alpha_2$ , and no correlation with  $\Delta$ .

$\Omega_c$	$f_c/\text{mHz}$	$\alpha_1$	$\alpha_2$	$\Delta$	$\Pi$
$6.072 \times 10^{-4}$	1.807	85	-87	46	0.9999

TABLE III: Parameter values for the broken power-law template (6) for the Nieh-Yan coupling model.

### B. Normalized model parameters

Based on the relationship between the spectral parameters and the physical parameters, the Eqs. (3) and (4) for the dark photon couplings, as well as Eqs. (7) and (8) for the Nieh-Yan coupling, which enables us to constrain the physical parameters via measurements of the spectral shape.

We introduce the dimensionless normalized model parameters by combining the axion mass  $m$ , the coupling constant  $\alpha_{X/T}$ , and the decay constant  $f_{X/T}$  as follows:

$$\tilde{m}_{X/T} = \frac{m}{\text{eV}} \left( \frac{\alpha_{X/T}}{M_P^2} \right)^{4/3}, \quad (31)$$

$$\tilde{f}_X = \frac{f_X}{M_P} \left( \frac{\alpha_X}{M_P^2} \right)^{-1/3}, \quad \tilde{f}_T = \frac{f_T}{M_P}, \quad (32)$$

and substitute them into the spectral form (2) and (6). From the specific physical parameters of the dark photon coupling and the Nieh-Yan coupling models, as described in Sec. II A and II B respectively, we obtain the values of these dimensionless normalized model parameters, which

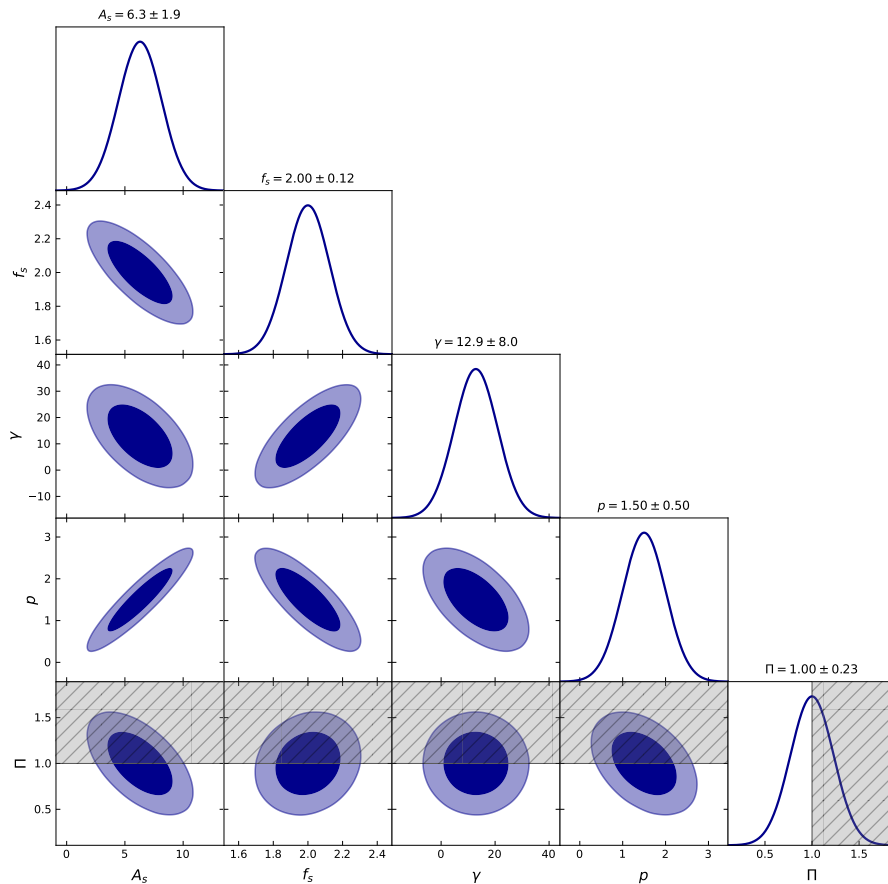


FIG. 5: Corner plots of SGWB spectral parameters estimates for the dark photon coupling model derived from the Fisher matrix, with parameter values listed in Table II. At the top of each column, the corresponding parameters'  $1\sigma$  uncertainty are presented. The gray shaded areas correspond to regions of the parameter space with  $\Pi > 1$ , which is theoretically unacceptable.

are explicitly listed in Table IV. We use the Fisher matrix to estimate the normalized model parameters.

We compute the Fisher matrix of the normalized model parameters  $\tilde{m}$ ,  $\tilde{f}_X$ , and  $\tilde{f}_T$  to obtain its covariance matrix. The correlation plots of this matrix are shown in Figs. 7a and 7b. We can constrain the values of the physical parameters by the measurement of these normalized model parameters.

For dark photon coupling model as given in Eq. (2), the results are shown in Fig. 7a. At the  $1\sigma$  confidence level, the relative errors are less than 6.7% for the normalized model parameters. It can be observed that the measurements of  $\tilde{m}_X$  and  $\tilde{f}_X$  are approximately independent, whereas  $\Pi$  exhibits a certain degree of negative correlation with both  $\tilde{m}_X$  and  $\tilde{f}_X$ . The parameter  $\Pi$  is estimated to be 0.9999 with a relative uncertainty of

21.0% at the  $1\sigma$  confidence level. To improve the measurement precision of  $\Pi$ , we can enhance the sensitivity of individual detectors and the detector network, as well as achieve higher SNR.

For the Nieh-Yan coupling model, the result for the broken power-law template in Eq. (6) is shown in Fig. 7b. At the  $1\sigma$  confidence level, the relative errors are less than 2.2% for the normalized model parameters. It can be observed that the measurements of the parameters  $\tilde{m}_T$ ,  $\tilde{f}_T$ , and  $\Pi$  are correlated. Moreover, due to the strong signal strength, the measurement precision of  $\Pi$  has been improved compared to the results for the dark photon coupling model, with a relative error of 6.2% at the  $1\sigma$  confidence level. Meanwhile, we can see that the measurement precision of  $\tilde{m}_T$  is relatively high. This is because the broken power-law template has a narrow peak

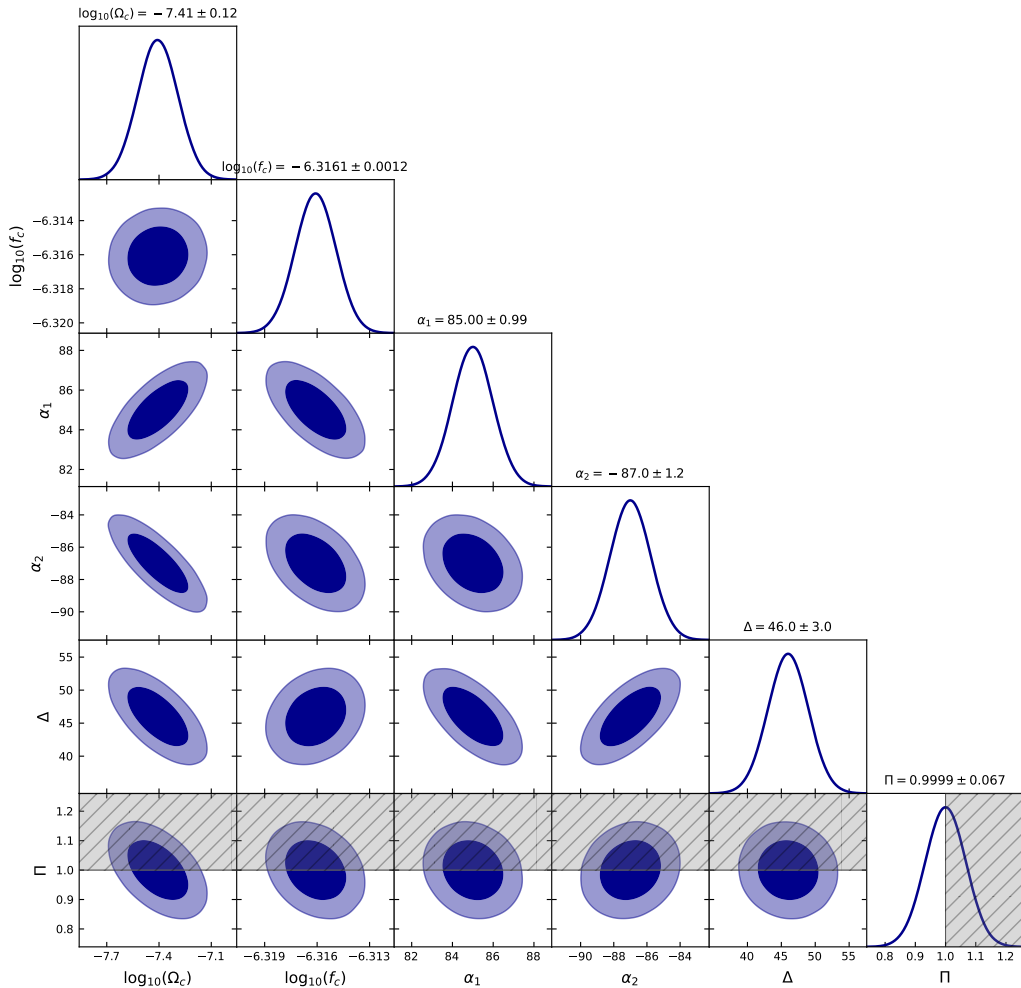
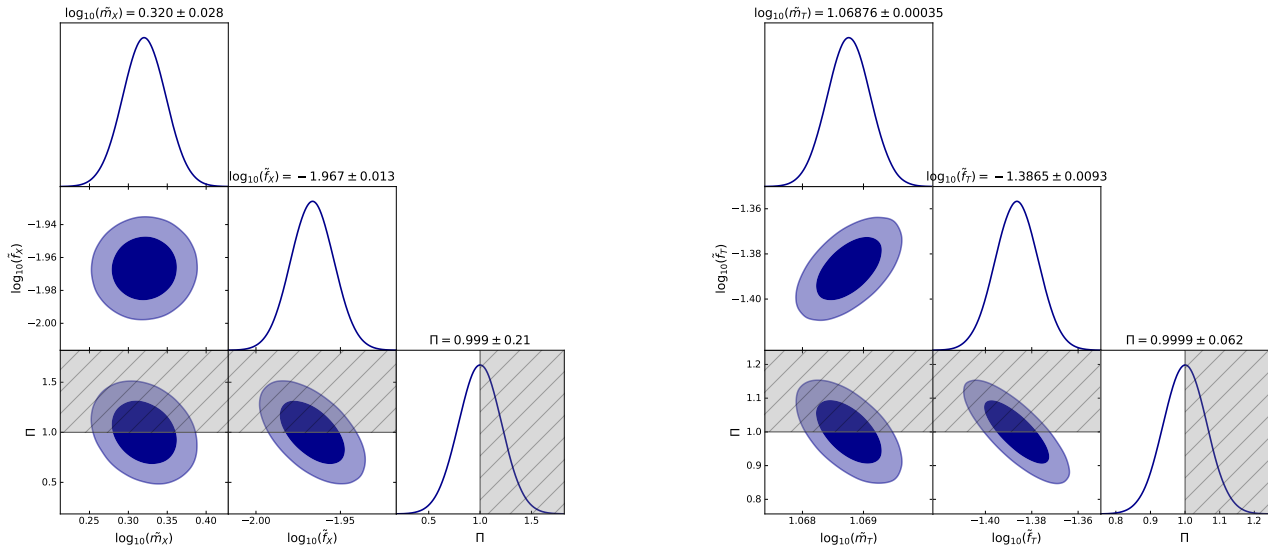


FIG. 6: Corner plots of SGWB spectral parameters estimates for the Nieh-Yan coupling model derived from the Fisher matrix, with parameter values listed in Table III. At the top of each column, the corresponding parameters'  $1\sigma$  uncertainty is presented. The gray shaded areas correspond to regions of the parameter space with  $\Pi > 1$ , which is theoretically unacceptable.

and strong amplitude at the peak frequency, measuring the peak frequency more sensitive. According to the relationships (7) and (31), it is clear that  $\tilde{m}$  corresponds to the measurement of the peak frequency.

$\mathcal{O}$	$\tilde{m}_{\mathcal{O}}$	$\tilde{f}_{\mathcal{O}}$	$\Pi$
$X$ (Dark Photon)	2.092	0.0108	0.9999
$T$ (Nieh-Yan)	11.72	0.0411	0.9999

TABLE IV: Values of the normalized model parameters for dark photon coupling and Nieh-Yan coupling models. The subscript  $\mathcal{O}$  in  $\tilde{m}_{\mathcal{O}}$  and  $\tilde{f}_{\mathcal{O}}$  denotes the model index:  $\mathcal{O} = X$  for dark photon coupling,  $\mathcal{O} = T$  for Nieh-Yan coupling.



(a) Normalized parameters in dark photon coupling model.

(b) Normalized parameters in Nieh-Yan coupling model.

FIG. 7: Corner plots showing SGWB normalized model parameters estimates from the Fisher matrix for (a) the dark photon coupling model and (b) the Nieh-Yan coupling model in Table IV. At the top of each column, the corresponding parameters'  $1\sigma$  uncertainties are presented. The gray shaded areas correspond to regions of the parameter space with  $\Pi > 1$  which is theoretically unacceptable.

## V. CONCLUSION

The single GW detectors face challenges in detecting the chirality of GWs due to their planar design. However, with the network of space-based detectors such as LISA and Taiji through cross-correlation techniques, we can compute chirality-dependent response functions and extract the net circular polarization of an isotropic SGWB. The detection of parity violation through chiral GWs is crucial for understanding the early Universe and for distinguishing a cosmological GW background from an astrophysical one [56]. In this work, we present the response functions for Stokes parameters  $I$  and  $V$ , as well as the total intensity sensitivity curve for GWBs originating from audible axions, using the LISA-Taiji network. In addition to the LISA-Taiji network, other space-based GW detector networks such as LISA-TianQin have also been proposed and studied extensively [95–98].

We use the Fisher information matrix to estimate both spectral parameters and normalized model parameters of axion-induced chiral GW spectra through the LISA-Taiji network, focusing on axion-dark photon and axion-Nieh-Yan couplings with physical parameters selected to yield strong GWs in the mHz range. Our results demonstrate that the network estimates the spectral shape parameters and normalized model parameters for both coupling models. For the spectral shape parameters in the dark photon coupling model, we obtain relative errors of 62.0%

at the  $1\sigma$  confidence level, while for the Nieh-Yan coupling model, the relative errors are less than 31.8% at the same confidence level. Regarding circular polarization parameter  $\Pi$ , its relative error is less than 23.0% ( $1\sigma$ ) for the dark photon coupling model, and it is reduced to 6.7% ( $1\sigma$ ) for the stronger signals from the Nieh-Yan coupling model. Compared to flat GW spectra in [56], we have computed the parameter uncertainties for frequency-dependent spectra of the axion-induced chiral GWB, demonstrating the LISA-Taiji network's capability to effectively constrain both GW spectral parameters and normalized model parameters.

## ACKNOWLEDGEMENT

This work is supported by the National Key Research and Development Program of China (No. 2023YFC2206200, No.2021YFC2201901) and the National Natural Science Foundation of China (No.12375059, No.1240507).

## Appendix A: Response functions of GWs

In this work, we employ natural units and adopt the Lorentz transverse-traceless gauge. We establish a coordinate system  $\{\hat{e}_x, \hat{e}_y, \hat{e}_z\}$  at rest relative to an isotropic SGWB.

## 1. Polarization tensor bases

For an incoming plane GW with a single wave vector  $\vec{k}$ , we define an orthogonal basis

$$\hat{u}(\hat{k}) = \frac{\hat{k} \times \hat{e}_z}{|\hat{k} \times \hat{e}_z|}, \quad \hat{v}(\hat{k}) = \hat{k} \times \hat{u}, \quad (\text{A1})$$

where  $\hat{k}$  denotes the unit vector in the direction of wave-vector  $\vec{k}$ , and its magnitude is given by  $k = |\vec{k}|$ . Using the above equation, we define the so-called ‘‘plus’’ (+) and ‘‘cross’’ ( $\times$ ) polarization tensors as

$$e_{ab}^+(\hat{k}) = \frac{\hat{u}_a \hat{u}_b - \hat{v}_a \hat{v}_b}{\sqrt{2}}, \quad e_{ab}^\times(\hat{k}) = \frac{\hat{u}_a \hat{v}_b + \hat{v}_a \hat{u}_b}{\sqrt{2}}. \quad (\text{A2})$$

It is more convenient to introduce the circular polarization basis tensors  $e_{ab}^R$  and  $e_{ab}^L$  when searching for evidence of circular polarization in the background. Then the relationships between the left- and right-handed polarization tensors and the ‘‘plus’’ (+) and ‘‘cross’’ ( $\times$ ) polarization basis are

$$e_{ab}^R(\hat{k}) = \frac{e_{ab}^+ + ie_{ab}^\times}{\sqrt{2}}, \quad e_{ab}^L(\hat{k}) = \frac{e_{ab}^+ - ie_{ab}^\times}{\sqrt{2}}. \quad (\text{A3})$$

The superposition of GWs arriving at position  $\vec{x}$  at time  $t$  can be represented as an incident plane wave

$$h_{ab}(\vec{x}, t) = \int_{-\infty}^{+\infty} df \int_{\Omega} d\Omega_{\hat{k}} e^{2\pi i f(t - \hat{k} \cdot \vec{x})} \sum_P \tilde{h}_P(f, \hat{k}) e_{ab}^P(\hat{k}), \quad (\text{A4})$$

where the index  $P$  labels either the plus and cross polarizations (+/ $\times$ ) or the left- and right-handed polarizations (L/R). Here,  $f = kc$  denotes the frequency of each plane wave,  $d\Omega_{\hat{k}}$  represents the infinitesimal solid angle corresponding to the wave vector  $\vec{k}$ , and  $\tilde{h}_P(f, \hat{k}) \equiv f^2 \tilde{h}_P(\vec{k})$ . Finally, the gravitational wave can be expressed in terms of  $\vec{k}$  as

$$h_{ab}(\vec{x}, t) = \int d^3k e^{-2\pi i \vec{k} \cdot \vec{x}} \sum_P \left[ e^{2\pi i kt} \tilde{h}_P(\vec{k}) e_{ab}^P(\hat{k}) + e^{-2\pi i kt} \tilde{h}_P^*(-\vec{k}) e_{ab}^{P*}(-\hat{k}) \right]. \quad (\text{A5})$$

## 2. Quadratic response functions

In actual measurements, space-based detectors measure differential Doppler frequency shifts rather than direct time shifts. These shifts are defined as  $\Delta F_{12}(t) \equiv \Delta \nu_{12}(t)/\nu = -d\Delta T_{12}(t)/dt$ . We use  $L$  to denote the detector arm length. The most straightforward interferometric measurement at a vertex performed by a space-based detector is

$$\Delta F_{1(23)}(t) = \Delta F_{21}(t-L) + \Delta F_{12}(t) - [\Delta F_{31}(t-L) + \Delta F_{13}(t)]. \quad (\text{A6})$$

In order to suppress noise induced by laser phase variations and other factors, we implement TDI techniques. Consider two test masses labeled  $i$  and  $j$ , and let  $\hat{l}_{ij} = (\mathbf{x}_j - \mathbf{x}_i)/|\mathbf{x}_j - \mathbf{x}_i|$  denote the unit vector pointing from mass  $i$  to mass  $j$  among the three detector spacecraft. The TDI1.5 variable is obtained through cyclic permutation of the TDI variables Y and Z

$$\begin{aligned} \Delta F_{1(23)}^{1.5}(t) &= \Delta F_{1(23)}(t-2L) + \Delta F_{1(32)}(t) \\ &= - \int d^3k e^{-2\pi i \vec{k} \cdot \vec{x}_1} (2\pi i k L) \times \\ &\quad \sum_{\lambda} \left[ e^{2\pi i k(t-L)} W(kL) R_1^{\lambda}(\vec{k}, \hat{l}_{12}, \hat{l}_{13}) \tilde{h}_{\lambda}(k) \right. \\ &\quad \left. - e^{-2\pi i k(t-L)} W^*(kL) R_1^{\lambda*}(-\vec{k}, \hat{l}_{12}, \hat{l}_{13}) \tilde{h}_{\lambda}^*(-k) \right]. \end{aligned} \quad (\text{A7})$$

where  $\lambda = L$  or  $R$  denotes left- and right-handed polarizations, and  $W(kL) \equiv e^{-4\pi i kL} - 1$ . The function  $R_i^{\lambda}$  is defined as

$$R_i^{\lambda}(\vec{k}, \hat{l}_{ij}, \hat{l}_{ik}) \equiv \frac{\hat{l}_{ij}^a \hat{l}_{ij}^b}{2} e_{ab}^{\lambda}(\hat{k}) \mathcal{T}(\vec{k}, \hat{l}_{ij}) - \frac{\hat{l}_{ik}^a \hat{l}_{ik}^b}{2} e_{ab}^{\lambda}(\hat{k}) \mathcal{T}(\vec{k}, \hat{l}_{ik}), \quad (\text{A8})$$

where the detector transfer function  $\mathcal{T}(\vec{k}, \hat{l}_{ij})$  is given by

$$\begin{aligned} \mathcal{T}(\vec{k}, \hat{l}_{ij}) &\equiv e^{\pi i k L(1 - \hat{k} \cdot \hat{l}_{ij})} \text{sinc} \left[ \pi k L \left( 1 + \hat{k} \cdot \hat{l}_{ij} \right) \right] \\ &\quad + e^{-\pi i k L(1 + \hat{k} \cdot \hat{l}_{ij})} \text{sinc} \left[ \pi k L \left( 1 - \hat{k} \cdot \hat{l}_{ij} \right) \right]. \end{aligned} \quad (\text{A9})$$

For simplicity, we represent the detector output using the notation  $s_i(t) \equiv \Delta F_{i(jk)}^{1.5}(t)$ . The information is contained within the two-point correlation functions of the data streams. Below, without assuming identical detectors, we present the general formulation. The two-point cross-correlation is expressed as

$$\begin{aligned} \langle s_i(t) s_j(t) \rangle &= \int dk (2\pi k L_i) (2\pi k L_j) \sum_{\lambda} P_{\lambda}(k) \times \\ &\quad \left[ e^{-2\pi i k(L_i - L_j)} W(kL_i) W^*(kL_j) \tilde{\Gamma}_{ij}^{\lambda}(k) + \text{h.c.} \right], \end{aligned} \quad (\text{A10})$$

where the cross-correlation function

$$\begin{aligned} \tilde{\Gamma}_{ij}^{\lambda}(k) &\equiv \frac{1}{4\pi} \int d^2\hat{k} e^{-2\pi i \vec{k} \cdot (\vec{x}_i - \vec{x}_j)} \\ &\quad \times R_i^{\lambda}(\vec{k}, \hat{l}_{ik}, \hat{l}_{il}) R_j^{\lambda*}(\vec{k}, \hat{l}_{jm}, \hat{l}_{jn}). \end{aligned} \quad (\text{A11})$$

For notational simplicity, the quadratic response function

$$\Gamma_{ij}^{\lambda}(k) \equiv (2\pi k L_i) (2\pi k L_j) W(kL_i) W^*(kL_j) \tilde{\Gamma}_{ij}^{\lambda}(k) + \text{h.c.}, \quad (\text{A12})$$

we obtain the compact form

$$\langle s_i(t) s_j(t) \rangle = \int dk \left[ \Gamma_{ij}^L(k) P_L(k) + \Gamma_{ij}^R(k) P_R(k) \right]. \quad (\text{A13})$$

When  $i$  and  $j$  are both LISA (or Taiji) channels, the response function is given by

$$\begin{aligned}\Gamma_{ij}(k) &= \Gamma_{ij}^L(k) + \Gamma_{ij}^R(k) \\ &= 16(2\pi kL)^2 \sin^2(2\pi kL) \tilde{\Gamma}_{ij}(k),\end{aligned}\quad (\text{A14})$$

where  $\tilde{\Gamma}_{ij}(k) = \tilde{\Gamma}_{ij}^L(k) = \tilde{\Gamma}_{ij}^R(k)$  [12]. The response functions  $\Gamma_{ij}$  for the A and E channels of LISA and Taiji are shown in Fig. 3a.

Using the methods in [56, 99], we have calculated the response functions and total intensity sensitivity curves associated with the self-correlation of LISA and Taiji. The corresponding results are shown in Fig. 3. Additionally, we have obtained the response functions for the  $I$  and  $V$  components of all cross-correlation TDI channels between LISA and Taiji, as shown in Fig. 4. For further details on the derivation, we refer to [12, 56].

### 3. The AET bases

In space-based gravitational wave detection, the fundamental TDI channels of a Michelson interferometer include X, Y, and Z. We transform the X, Y, and Z channels into the noise-independent channels A, E, and T, which

are related as follows [56]

$$\tilde{d}_A = \frac{1}{\sqrt{2}}(\tilde{d}_Z - \tilde{d}_X), \quad (\text{A15})$$

$$\tilde{d}_E = \frac{1}{\sqrt{6}}(\tilde{d}_X - 2\tilde{d}_Y + \tilde{d}_Z), \quad (\text{A16})$$

$$\tilde{d}_T = \frac{1}{\sqrt{3}}(\tilde{d}_X + \tilde{d}_Y + \tilde{d}_Z). \quad (\text{A17})$$

The noise independence of the A, E, and T channels is valid under the assumptions of identical noise in each laser link and equal arm lengths.

For convenience, we summarize the key symbols used in this paper in Table V.

Symbols	Descriptions
$S_{ij}(f)$	One-sided signal PSD
$N_i(f)$	One-sided noise PSD
$h_{ab}(\vec{x}, t)$	Gravitational wave strain tensor
$\Delta F_{ij}(t)$	Doppler frequency shifts
$\tilde{\Gamma}_{ij}^\lambda(k)$	Cross-correlation function
$\Gamma_{ij}^\lambda(k)$	Quadratic response function

TABLE V: Summary of the symbols and descriptions.

- 
- [1] B. P. Abbott *et al.* (LIGO Scientific, Virgo), Observation of Gravitational Waves from a Binary Black Hole Merger, *Phys. Rev. Lett.* **116**, 061102 (2016), [arXiv:1602.03837 \[gr-qc\]](#).
- [2] A. Abramovici *et al.*, LIGO: The Laser interferometer gravitational wave observatory, *Science* **256**, 325 (1992).
- [3] B. Allen, The Stochastic gravity wave background: Sources and detection, in *Les Houches School of Physics: Astrophysical Sources of Gravitational Radiation* (1996) pp. 373–417, [arXiv:gr-qc/9604033](#).
- [4] M. Maggiore, Gravitational wave experiments and early universe cosmology, *Phys. Rept.* **331**, 283 (2000), [arXiv:gr-qc/9909001](#).
- [5] S. Kuroyanagi, T. Chiba, and T. Takahashi, Probing the Universe through the Stochastic Gravitational Wave Background, *JCAP* **11**, 038, [arXiv:1807.00786 \[astro-ph.CO\]](#).
- [6] P. Auclair *et al.* (LISA Cosmology Working Group), Cosmology with the Laser Interferometer Space Antenna, *Living Rev. Rel.* **26**, 5 (2023), [arXiv:2204.05434 \[astro-ph.CO\]](#).
- [7] P. Binetruy, A. Bohe, C. Caprini, and J.-F. Dufaix, Cosmological Backgrounds of Gravitational Waves and eLISA/NGO: Phase Transitions, Cosmic Strings and Other Sources, *JCAP* **06**, 027, [arXiv:1201.0983 \[gr-qc\]](#).
- [8] E. Thrane and J. D. Romano, Sensitivity curves for searches for gravitational-wave backgrounds, *Phys. Rev. D* **88**, 124032 (2013), [arXiv:1310.5300 \[astro-ph.IM\]](#).
- [9] J. D. Romano and N. J. Cornish, Detection methods for stochastic gravitational-wave backgrounds: a unified treatment, *Living Rev. Rel.* **20**, 2 (2017), [arXiv:1608.06889 \[gr-qc\]](#).
- [10] C. Caprini and D. G. Figueroa, Cosmological Backgrounds of Gravitational Waves, *Class. Quant. Grav.* **35**, 163001 (2018), [arXiv:1801.04268 \[astro-ph.CO\]](#).
- [11] G. Boileau, N. Christensen, R. Meyer, and N. J. Cornish, Spectral separation of the stochastic gravitational-wave background for LISA: Observing both cosmological and astrophysical backgrounds, *Phys. Rev. D* **103**, 103529 (2021), [arXiv:2011.05055 \[gr-qc\]](#).
- [12] R. Flauger, N. Karnesis, G. Nardini, M. Pieroni, A. Ricciardone, and J. Torrado, Improved reconstruction of a stochastic gravitational wave background with LISA, *JCAP* **01**, 059, [arXiv:2009.11845 \[astro-ph.CO\]](#).
- [13] N. van Remortel, K. Janssens, and K. Turbang, Stochastic gravitational wave background: Methods and implications, *Prog. Part. Nucl. Phys.* **128**, 104003 (2023), [arXiv:2210.00761 \[gr-qc\]](#).
- [14] R. D. Peccei and H. R. Quinn, CP Conservation in the Presence of Instantons, *Phys. Rev. Lett.* **38**, 1440 (1977).
- [15] R. D. Peccei and H. R. Quinn, Constraints Imposed by CP Conservation in the Presence of Instantons, *Phys. Rev. D* **16**, 1791 (1977).
- [16] S. Weinberg, A New Light Boson?, *Phys. Rev. Lett.* **40**, 223 (1978).
- [17] F. Wilczek, Problem of Strong  $P$  and  $T$  Invariance in the

- Presence of Instantons, *Phys. Rev. Lett.* **40**, 279 (1978).
- [18] N. Du *et al.* (ADMX), A Search for Invisible Axion Dark Matter with the Axion Dark Matter Experiment, *Phys. Rev. Lett.* **120**, 151301 (2018), [arXiv:1804.05750 \[hep-ex\]](#).
- [19] L. Di Luzio, M. Giannotti, E. Nardi, and L. Visinelli, The landscape of QCD axion models, *Phys. Rept.* **870**, 1 (2020), [arXiv:2003.01100 \[hep-ph\]](#).
- [20] L. F. Abbott and P. Sikivie, A Cosmological Bound on the Invisible Axion, *Phys. Lett. B* **120**, 133 (1983).
- [21] J. Ipser and P. Sikivie, Are Galactic Halos Made of Axions?, *Phys. Rev. Lett.* **50**, 925 (1983).
- [22] D. J. E. Marsh, Axion Cosmology, *Phys. Rept.* **643**, 1 (2016), [arXiv:1510.07633 \[astro-ph.CO\]](#).
- [23] J. Preskill, M. B. Wise, and F. Wilczek, Cosmology of the Invisible Axion, *Phys. Lett. B* **120**, 127 (1983).
- [24] P. Sikivie, Experimental Tests of the Invisible Axion, *Phys. Rev. Lett.* **51**, 1415 (1983), [Erratum: *Phys. Rev. Lett.* **52**, 695 (1984)].
- [25] H. Georgi, H. R. Quinn, and S. Weinberg, Hierarchy of Interactions in Unified Gauge Theories, *Phys. Rev. Lett.* **33**, 451 (1974).
- [26] P. W. Graham, D. E. Kaplan, and S. Rajendran, Cosmological Relaxation of the Electroweak Scale, *Phys. Rev. Lett.* **115**, 221801 (2015), [arXiv:1504.07551 \[hep-ph\]](#).
- [27] M. Dine and W. Fischler, The not-so-harmless axion, *Physics Letters B* **120**, 137 (1983).
- [28] G. Bertone and D. Hooper, History of dark matter, *Rev. Mod. Phys.* **90**, 045002 (2018), [arXiv:1605.04909 \[astro-ph.CO\]](#).
- [29] K. Freese, J. A. Frieman, and A. V. Olinto, Natural inflation with pseudo - Nambu-Goldstone bosons, *Phys. Rev. Lett.* **65**, 3233 (1990).
- [30] A. Arvanitaki, S. Dimopoulos, S. Dubovsky, N. Kaloper, and J. March-Russell, String Axiverse, *Phys. Rev. D* **81**, 123530 (2010), [arXiv:0905.4720 \[hep-th\]](#).
- [31] C. S. Machado, W. Ratzinger, P. Schwaller, and B. A. Stefanek, Audible Axions, *JHEP* **01**, 053, [arXiv:1811.01950 \[hep-ph\]](#).
- [32] E. Madge, W. Ratzinger, D. Schmitt, and P. Schwaller, Audible axions with a booster: Stochastic gravitational waves from rotating ALPs, *SciPost Phys.* **12**, 171 (2022), [arXiv:2111.12730 \[hep-ph\]](#).
- [33] A. Lue, L.-M. Wang, and M. Kamionkowski, Cosmological signature of new parity violating interactions, *Phys. Rev. Lett.* **83**, 1506 (1999), [arXiv:astro-ph/9812088](#).
- [34] K. Nagano, T. Fujita, Y. Michimura, and I. Obata, Axion Dark Matter Search with Interferometric Gravitational Wave Detectors, *Phys. Rev. Lett.* **123**, 111301 (2019), [arXiv:1903.02017 \[hep-ph\]](#).
- [35] J. Heinze, A. Gill, A. Dmitriev, J. Smetana, T. Yan, V. Boyer, D. Martynov, and M. Evans, First Results of the Laser-Interferometric Detector for Axions (LIDA), *Phys. Rev. Lett.* **132**, 191002 (2024), [arXiv:2307.01365 \[astro-ph.CO\]](#).
- [36] Y.-H. Yao and Y. Tang, Probing stochastic ultra-light dark matter with space-based gravitational-wave interferometers, *Phys. Rev. D* **110**, 095015 (2024), [arXiv:2404.01494 \[hep-ph\]](#).
- [37] J. Gué, A. Hees, and P. Wolf, Probing the axion-photon coupling with space-based gravitational wave detectors, *Class. Quant. Grav.* **42**, 055015 (2025), [arXiv:2410.17763 \[hep-ph\]](#).
- [38] Y.-H. Yao, T. Jiang, and Y. Tang, Prospects for Axion Dark Matter Searches at LISA-like Interferometers, *arXiv preprint* (2024), [arXiv:2410.22072 \[hep-ph\]](#).
- [39] N. Christensen, Stochastic Gravitational Wave Backgrounds, *Rept. Prog. Phys.* **82**, 016903 (2019), [arXiv:1811.08797 \[gr-qc\]](#).
- [40] B. Allen and J. D. Romano, Detecting a stochastic background of gravitational radiation: Signal processing strategies and sensitivities, *Phys. Rev. D* **59**, 102001 (1999), [arXiv:gr-qc/9710117](#).
- [41] R. Jackiw and S. Y. Pi, Chern-Simons modification of general relativity, *Phys. Rev. D* **68**, 104012 (2003), [arXiv:gr-qc/0308071](#).
- [42] S. Alexander and N. Yunes, Chern-Simons Modified General Relativity, *Phys. Rept.* **480**, 1 (2009), [arXiv:0907.2562 \[hep-th\]](#).
- [43] M. Li, H. Rao, and D. Zhao, A simple parity violating gravity model without ghost instability, *JCAP* **11**, 023, [arXiv:2007.08038 \[gr-qc\]](#).
- [44] M. Li, H. Rao, and Y. Tong, Revisiting a parity violating gravity model without ghost instability: Local Lorentz covariance, *Phys. Rev. D* **104**, 084077 (2021), [arXiv:2104.05917 \[gr-qc\]](#).
- [45] R.-G. Cai, C. Fu, and W.-W. Yu, Parity violation in stochastic gravitational wave background from inflation in Nieh-Yan modified teleparallel gravity, *Phys. Rev. D* **105**, 103520 (2022), [arXiv:2112.04794 \[astro-ph.CO\]](#).
- [46] Q. Wu, T. Zhu, R. Niu, W. Zhao, and A. Wang, Constraints on the Nieh-Yan modified teleparallel gravity with gravitational waves, *Phys. Rev. D* **105**, 024035 (2022), [arXiv:2110.13870 \[gr-qc\]](#).
- [47] M. Li and H. Rao, Irregular universe in the Nieh-Yan modified teleparallel gravity, *Phys. Lett. B* **841**, 137929 (2023), [arXiv:2301.02847 \[gr-qc\]](#).
- [48] M. Li, Y. Tong, and D. Zhao, Possible consistent model of parity violations in the symmetric teleparallel gravity, *Phys. Rev. D* **105**, 104002 (2022), [arXiv:2203.06912 \[gr-qc\]](#).
- [49] H. Rao and D. Zhao, Parity violating scalar-tensor model in teleparallel gravity and its cosmological application, *JHEP* **08**, 070, [arXiv:2304.07138 \[gr-qc\]](#).
- [50] F. Zhang, J.-X. Feng, and X. Gao, Scalar induced gravitational waves in metric teleparallel gravity with the Nieh-Yan term, *Phys. Rev. D* **110**, 023537 (2024), [arXiv:2404.02922 \[gr-qc\]](#).
- [51] B. Xu, K. Ding, H. Su, J. Chen, and Y.-L. Zhang, Chiral Gravitational Wave Background from Audible Axion via Nieh-Yan Term, *arXiv preprint* (2024), [arXiv:2411.08691 \[hep-ph\]](#).
- [52] N. Seto and A. Taruya, Measuring a Parity Violation Signature in the Early Universe via Ground-based Laser Interferometers, *Phys. Rev. Lett.* **99**, 121101 (2007), [arXiv:0707.0535 \[astro-ph\]](#).
- [53] N. Seto and A. Taruya, Polarization analysis of gravitational-wave backgrounds from the correlation signals of ground-based interferometers: Measuring a circular-polarization mode, *Phys. Rev. D* **77**, 103001 (2008), [arXiv:0801.4185 \[astro-ph\]](#).
- [54] T. L. Smith and R. Caldwell, Sensitivity to a Frequency-Dependent Circular Polarization in an Isotropic Stochastic Gravitational Wave Background, *Phys. Rev. D* **95**, 044036 (2017), [arXiv:1609.05901 \[gr-qc\]](#).
- [55] N. Seto, Prospects for direct detection of circular polarization of gravitational-wave background, *Phys. Rev. Lett.* **97**, 151101 (2006), [arXiv:astro-ph/0609504](#).

- [56] G. Orlando, M. Pieroni, and A. Ricciardone, Measuring Parity Violation in the Stochastic Gravitational Wave Background with the LISA-Taiji network, *JCAP* **03**, 069, [arXiv:2011.07059 \[astro-ph.CO\]](#).
- [57] S. Saito, K. Ichiki, and A. Taruya, Probing polarization states of primordial gravitational waves with CMB anisotropies, *JCAP* **09**, 002, [arXiv:0705.3701 \[astro-ph\]](#).
- [58] L. Sorbo, Parity violation in the Cosmic Microwave Background from a pseudoscalar inflaton, *JCAP* **06**, 003, [arXiv:1101.1525 \[astro-ph.CO\]](#).
- [59] P. Amaro-Seoane *et al.* (LISA), Laser Interferometer Space Antenna, arXiv preprint (2017), [arXiv:1702.00786 \[astro-ph.IM\]](#).
- [60] W.-H. Ruan, Z.-K. Guo, R.-G. Cai, and Y.-Z. Zhang, Taiji program: Gravitational-wave sources, *Int. J. Mod. Phys. A* **35**, 2050075 (2020), [arXiv:1807.09495 \[gr-qc\]](#).
- [61] N. Seto, Correlation analysis of stochastic gravitational wave background around 0.1-1 Hz, *Phys. Rev. D* **73**, 063001 (2006), [arXiv:gr-qc/0510067](#).
- [62] B. Abbott *et al.* (LIGO Scientific), Searching for a Stochastic Background of Gravitational Waves with LIGO, *Astrophys. J.* **659**, 918 (2007), [arXiv:astro-ph/0608606](#).
- [63] B. F. Schutz, Networks of gravitational wave detectors and three figures of merit, *Class. Quant. Grav.* **28**, 125023 (2011), [arXiv:1102.5421 \[astro-ph.IM\]](#).
- [64] N. Seto, Measuring Parity Asymmetry of Gravitational Wave Backgrounds with a Heliocentric Detector Network in the mHz Band, *Phys. Rev. Lett.* **125**, 251101 (2020), [arXiv:2009.02928 \[gr-qc\]](#).
- [65] W.-H. Ruan, C. Liu, Z.-K. Guo, Y.-L. Wu, and R.-G. Cai, The LISA-Taiji network, *Nature Astron.* **4**, 108 (2020), [arXiv:2002.03603 \[gr-qc\]](#).
- [66] G. Wang, W.-T. Ni, W.-B. Han, P. Xu, and Z. Luo, Alternative LISA-TAIJI networks, *Phys. Rev. D* **104**, 024012 (2021), [arXiv:2105.00746 \[gr-qc\]](#).
- [67] G. Wang and W.-B. Han, Alternative LISA-TAIJI networks: Detectability of the isotropic stochastic gravitational wave background, *Phys. Rev. D* **104**, 104015 (2021), [arXiv:2108.11151 \[gr-qc\]](#).
- [68] R.-G. Cai, Z.-K. Guo, B. Hu, C. Liu, Y. Lu, W.-T. Ni, W.-H. Ruan, N. Seto, G. Wang, and Y.-L. Wu, On networks of space-based gravitational-wave detectors, *Fund. Res.* **4**, 1072 (2024), [arXiv:2305.04551 \[gr-qc\]](#).
- [69] Z.-C. Zhao and S. Wang, Measuring the anisotropies in astrophysical and cosmological gravitational-wave backgrounds with Taiji and LISA networks, *Sci. China Phys. Mech. Astron.* **67**, 120411 (2024), [arXiv:2407.09380 \[gr-qc\]](#).
- [70] J. Chen, C. Liu, and Y.-L. Zhang, Parity-violating Gravitational Wave Background Search with a Network of Space-borne Triangular Detectors, arXiv (2024), [arXiv:2410.18916 \[gr-qc\]](#).
- [71] G. Wang and W.-B. Han, Observing gravitational wave polarizations with the LISA-TAIJI network, *Phys. Rev. D* **103**, 064021 (2021), [arXiv:2101.01991 \[gr-qc\]](#).
- [72] X.-H. Zhang, S.-D. Zhao, S. D. Mohanty, and Y.-X. Liu, Resolving Galactic binaries using a network of space-borne gravitational wave detectors, *Phys. Rev. D* **106**, 102004 (2022), [arXiv:2206.12083 \[gr-qc\]](#).
- [73] C. Zhang, Y. Gong, and C. Zhang, Source localizations with the network of space-based gravitational wave detectors, *Phys. Rev. D* **106**, 024004 (2022), [arXiv:2112.02299 \[gr-qc\]](#).
- [74] K. J. Shuman and N. J. Cornish, Massive black hole binaries and where to find them with dual detector networks, *Phys. Rev. D* **105**, 064055 (2022), [arXiv:2105.02943 \[gr-qc\]](#).
- [75] W.-H. Ruan, C. Liu, Z.-K. Guo, Y.-L. Wu, and R.-G. Cai, The LISA-Taiji Network: Precision Localization of Coalescing Massive Black Hole Binaries, *Research* **2021**, 6014164 (2021), [arXiv:1909.07104 \[gr-qc\]](#).
- [76] Y. Yang, W.-B. Han, Q. Yun, P. Xu, and Z. Luo, Tracing astrophysical black hole seeds and primordial black holes with LISA-Taiji network, *Mon. Not. Roy. Astron. Soc.* **512**, 6217 (2022), [arXiv:2205.00408 \[gr-qc\]](#).
- [77] J. Chen, C.-S. Yan, Y.-J. Lu, Y.-T. Zhao, and J.-Q. Ge, On detecting stellar binary black holes via the LISA-Taiji network, *Res. Astron. Astrophys.* **21**, 285 (2021), [arXiv:2201.12516 \[astro-ph.HE\]](#).
- [78] T. Yang, Gravitational-Wave Detector Networks: Standard Sirens on Cosmology and Modified Gravity Theory, *JCAP* **05**, 044, [arXiv:2103.01923 \[astro-ph.CO\]](#).
- [79] L.-F. Wang, S.-J. Jin, J.-F. Zhang, and X. Zhang, Forecast for cosmological parameter estimation with gravitational-wave standard sirens from the LISA-Taiji network, *Sci. China Phys. Mech. Astron.* **65**, 210411 (2022), [arXiv:2101.11882 \[gr-qc\]](#).
- [80] R. Wang, W.-H. Ruan, Q. Yang, Z.-K. Guo, R.-G. Cai, and B. Hu, Hubble parameter estimation via dark sirens with the LISA-Taiji network, *Natl. Sci. Rev.* **9**, nwab054 (2022), [arXiv:2010.14732 \[astro-ph.CO\]](#).
- [81] C. S. Machado, W. Ratzinger, P. Schwaller, and B. A. Stefanek, Gravitational wave probes of axionlike particles, *Phys. Rev. D* **102**, 075033 (2020), [arXiv:1912.01007 \[hep-ph\]](#).
- [82] B. Salehian, M. A. Gorji, S. Mukohyama, and H. Firouzjahi, Analytic study of dark photon and gravitational wave production from axion, *JHEP* **05**, 043, [arXiv:2007.08148 \[hep-ph\]](#).
- [83] S. Sun and Y.-L. Zhang, Fast gravitational wave bursts from axion clumps, *Phys. Rev. D* **104**, 103009 (2021), [arXiv:2003.10527 \[hep-ph\]](#).
- [84] M. Li, S. Sun, Q.-S. Yan, and Z. Zhao, Gravitational waves from axion wave production, *Eur. Phys. J. C* **84**, 1165 (2024), [arXiv:2309.08407 \[hep-ph\]](#).
- [85] K. Ding, C. Fu, B. Xu, and Y.-L. Zhang, Chiral gravitational wave background in millihertz from axion-like fields, *SCIENTIA SINICA Physica, Mechanica, Astronomica* **54**, 270408 (2024).
- [86] S. Babak and A. Petiteau, *LISA Data Challenge Manual*, Tech. Rep. LISA-LCST-SGS-MAN-002 (APC Paris, 2020).
- [87] M. Armano *et al.*, Sub-Femto- g Free Fall for Space-Based Gravitational Wave Observatories: LISA Pathfinder Results, *Phys. Rev. Lett.* **116**, 231101 (2016).
- [88] S. Babak, A. Petiteau, and M. Hewitson, LISA Sensitivity and SNR Calculations, arXiv (2021), [arXiv:2108.01167 \[astro-ph.IM\]](#).
- [89] Z. Luo, Z. Guo, G. Jin, Y. Wu, and W. Hu, A brief analysis to Taiji: Science and technology, *Results Phys.* **16**, 102918 (2020).
- [90] Z. Luo, Y. Wang, Y. Wu, W. Hu, and G. Jin, The Taiji program: A concise overview, *PTEP* **2021**, 05A108 (2021).
- [91] T. A. Prince, M. Tinto, S. L. Larson, and J. W. Armstrong, The LISA optimal sensitivity, *Phys. Rev. D* **66**, 122002 (2002), [arXiv:gr-qc/0209039](#).

- [92] J. Chen, C. Liu, Y.-L. Zhang, and G. Wang, Alternative LISA-TAIJI networks: Detectability of the Parity Violation in Stochastic Gravitational Wave Background, arXiv preprint (2024), [arXiv:2412.18420 \[gr-qc\]](#).
- [93] N. J. Cornish and S. L. Larson, Space missions to detect the cosmic gravitational wave background, *Class. Quant. Grav.* **18**, 3473 (2001), [arXiv:gr-qc/0103075](#).
- [94] N. J. Cornish, Detecting a stochastic gravitational wave background with the Laser Interferometer Space Antenna, *Phys. Rev. D* **65**, 022004 (2002), [arXiv:gr-qc/0106058](#).
- [95] Y. Gong, J. Luo, and B. Wang, Concepts and status of Chinese space gravitational wave detection projects, *Nature Astron.* **5**, 881 (2021), [arXiv:2109.07442 \[astro-ph.IM\]](#).
- [96] E.-K. Li *et al.*, GWSpace: a multi-mission science data simulator for space-based gravitational wave detection, arXiv preprint (2023), [arXiv:2309.15020 \[gr-qc\]](#).
- [97] J. Wu and J. Li, Subtraction of the confusion foreground and parameter uncertainty of resolvable galactic binaries on the networks of space-based gravitational-wave detectors, *Phys. Rev. D* **108**, 124047 (2023), [arXiv:2307.05568 \[gr-qc\]](#).
- [98] J. Luo *et al.*, Fundamental Physics and Cosmology with TianQin, arXiv preprint (2025), [arXiv:2502.20138 \[gr-qc\]](#).
- [99] T. Robson, N. J. Cornish, and C. Liu, The construction and use of LISA sensitivity curves, *Class. Quant. Grav.* **36**, 105011 (2019), [arXiv:1803.01944 \[astro-ph.HE\]](#).